# New Self-Isolated MIMO Antenna Array for 5G mm-Wave Applications

Oludayo Sokunbi, Hussein Attia, *Member, IEEE*, Abubakar Hamza, *Studnet Member, IEEE*, Atif Shamim, *Senior Member, IEEE*, Yiyang Yu, and Ahmed A. Kishk, *Life Fellow, IEEE*.

***Abstract*—In this paper, a simple novel technique to self-isolate multiple-input-multiple-output (MIMO) antenna array elements for mm-wave applications is proposed. MIMO antenna arrays with inter-element separation of 0.2 mm (0.023$\lambda$ at 35 GHz) and measured high isolation (>50 dB) are presented. Several rigorously optimized slots of different shapes, positions, and dimensions are etched on the radiating patch to enhance the inter-element isolation within 28-37.5 GHz impedance bandwidth. The surface current distributions, parametric analysis, and two MIMO array configurations are employed to validate the proposed self-isolation technique. The novel mm-wave antenna exhibits high impedance bandwidth (>29%), high isolation (>50 dB), high efficiency (>90%), high gain (>9.5 dB), and low envelope correlation coefficient (<0.005) throughout the desired bandwidth. Two configurations of the MIMO antenna arrays are fabricated and measured to validate the simulation outcomes. To the best of the authors' knowledge, the presented design is the first to exhibit such wideband isolation improvement without any external decoupling structure at the mm-wave frequency range.**

***Index Terms*—Self-isolated antenna, mm-waves, multiple-input-multiple-output (MIMO), 5G Antennas.**

## I. Introduction

The 5G wireless technology offers high data rate, low latency, low energy and cost, increased spectral efficiency and channel capacity, especially when used in MIMO technology [1] - [2]. Therefore, mm-wave antenna arrays are explored to meet the user requirements of high throughput, with a very close distance between antenna elements to enable miniaturization [3]. However, antenna arrays design at mm-wave bands has been a growing concern among antenna engineers because of the inevitable, undesired mutual coupling between the antenna elements [4].

Various techniques have been reported in the literature to mitigate mutual coupling at mm-wave bands [5] - [20]. The defective fractal ground was reported by [5] to achieve 13 dB isolation improvement between two compact patch antenna arrays in the 11.4-11.78 GHz range. Metasurfaces have been used to achieve a maximum of 15 dB isolation improvement within 27-32 GHz in [6]. A maximum of 31.5 dB mutual coupling reduction at 60.4 GHz was achieved in [7] using metasurface shield. The authors in [8] proposed Complementary Split Ring Resonator (CSRR) as a decoupling element in a MIMO array to achieve 31.8 dB isolation improvement and improved the radiation characteristics within 24.7-25.3 GHz. Defected Ground Surfaces (DGS) [9] were used to enhance the isolation of two integrated antenna systems by 3 dB in the dual-band of 4G (3.8 and 5.5 GHz), and 5 dB in the 5G bands (24.4-29.3 GHz). Frequency Selective Surfaces (FSS) was reported to increase the isolation of a dielectric resonator (DRA) MIMO antenna by a maximum of 30 dB in the 57-63 GHz bandwidth [10]. In [11], a hybrid isolator was used as an EBG unit cell to improve the isolation of a MIMO dielectric resonator antenna by a maximum of 25 dB within 59.3-64.8 GHz impedance bandwidth. The authors in [12] have used metallic vias as a decoupling mechanism to achieve about 19.8 dB isolation improvement in the E-plane, and 22.7 dB in the H-plane of a $1\times2$ MIMO DRA antenna at 26 GHz. Metal strips were printed on a MIMO DRA to achieve a maximum isolation improvement of 12 dB in the 27.5-28.35 GHz [13]. The authors in [15] used multiple notches structures on the ground planes of a MIMO Vivaldi antenna to achieve 37.3 dB maximum mutual coupling reduction enhancement within 24.55-28.5 GHz. The feed line structure of a 56.5-64 GHz slot patch antenna was modified to achieve 38.6 dB maximum isolation improvement [16]. Several Electromagnetic Band Gap (EBG) surfaces were employed as decoupling structures in [17] - [19]. Defective Ground Surface (DGS) was used by [20] to decouple a slot-array patch antenna by 50 dB between 1.2-1.35 GHz.

Recently, antenna engineers have been considering inherently isolated MIMO antennas which do not require additional isolating structures. These antennas are more compact with reduced complexity and cost [21] - [29]. Some literature have discussed self-isolated antennas. In [21], a slot rotated at 45° was utilized between a substrate integrated waveguide with two-edged shorted vias to achieve maximum isolation, efficiency, and ECC of 18.5 dB, 79.2% and 0.02, respectively, over the 3.45-3.55 GHz. Y. Li *et al* [22] proposed an eight open-slot MIMO antenna array for smartphones over 3.4-3.6 GHz with isolation greater than 17.5 dB. Moreover, MIMO patch antennas for mobile phones with mutual coupling less than 17 dB over 3.4-3.6 GHz was reported in [23].

This paper presents a simple self-isolated MIMO antenna array at the 5G mm-wave frequency band for the first time. A tightly spaced patch antenna array with a maximum isolation improvement of 35 dB over the 28-37.5 GHz mm-wave frequency band is achieved. The impedance bandwidth and isolation improvements are enabled by meticulously introducing U-slot, H-slot, and five circular slots on the patch; which

Oludayo Sokunbi and Ahmed Kishk are with Electrical and Computer Engineering Dept, Concordia University, QC H4B 1R6, Canada.

Hussein Attia, and Abubakar Hamza are with the Center for Communication Systems and Sensing, and the Electrical Engineering Department at King Fahd University of Petroleum Minerals (KFUPM), Dhahran, 31261, Saudi Arabia.

Atif Shamim and Yiyang Yu are with Computer, Electrical, Mathematical Science and Engineering Division, King Abdullah University of Science and Technology (KAUST), Saudi Arabia.

are illustrated by studying the surface current distributions. The authors believe that this is the first time such concept is reported at the mm-wave frequency band of 28 GHz. 1×2 and 1×4 MIMO antenna arrays are presented to validate the proposed novel isolation mechanism. The proposed antenna exhibits high gain, efficiency, low correlation coefficient, and good radiation properties throughout the working bandwidth. The proposed highly isolated antenna is fabricated and tested.

The manuscript is organized as follows: Section II describes the antenna structure, which includes the evolution (i.e., development stages) of the proposed antenna array, the concept of wideband self-isolation, and the parametric analyses. Section III illustrates a 4-element antenna array to verify the MIMO capability of the proposed antenna, while Section IV concludes the paper.

## II. Antenna Structure and Development

In this Section, the antenna array design methodology is firstly discussed. Then, the self-isolation mechanism is thoroughly explained through the surface current distributions and S-parameters results. Rigorous parametric analyses are also presented to optimize the MIMO antenna performance. Finally, the far-field results are presented and discussed.

### A. Antenna Design and Evolution

Figure 1 depicts the evolution of the proposed antenna from a simple reference antenna (Ref. A) to the proposed antenna. Each antenna in Fig. 1 consists of two copper patches each with 0.035 mm thickness, mounted on Rogers RT5870 substrate of dielectric constant 2.33, loss tangent 0.0012, height 0.508 mm, and a total size of 19x12 $mm^2$. The patch dimensions are accurately designed to operate at the mm-wave frequency band of 28 GHz. The two antennas are placed side-by-side along the x-axis (H-plane) with an edge-to-edge distance of 0.2 mm. The two patches are fed with 50 Ω microstrip lines, each line with optimized dimensions of 1.11 mm x 3.9 mm and located at $L_{12}$ = 2.86 mm (See Fig. 2).

From Fig. 1, to realize the proposed antenna with wide bandwidth and improved isolation between the elements, a design evolution is performed where the initial reference antenna is denoted as Ref. A. Then, a U-slot is etched on the Ref. A antenna to form the Ref. B antenna. Another H-slot is etched on the Ref. B antenna to form the Ref. C antenna. Finally, five circular slots are etched on the Ref. C antenna to realize the proposed structure.

The circular slots have a diameter $d_1$= 0.78 mm, while the rectangular slots have a thickness $L_{14}$= 0.25 mm. The five circular slots are separated from each other by $d_2$= 0.45 mm and tilted by $c$ = 5.4°. The effect of the different slot shapes on the bandwidth improvement and isolation enhancement of the antenna is thoroughly explained in the subsequent sections. Fig. 2 depicts the detailed optimized structure and dimensions of the proposed antenna. Table I shows the dimensions of the proposed antenna.

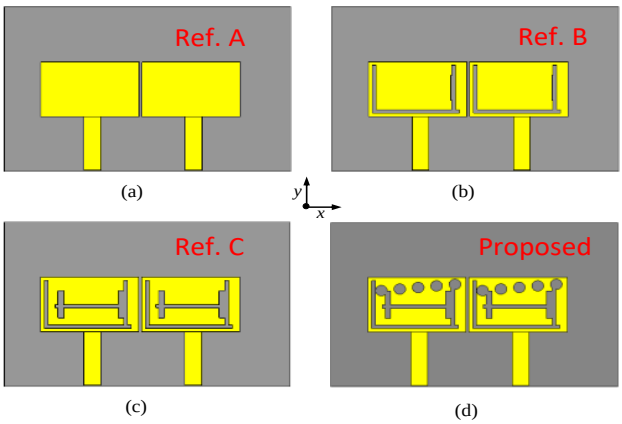


Fig. 1: Design evolution of the proposed 1×2 antenna array: (a) No slots (Ref. A) (b) Ref. A with U-slot (Ref. B) (c) Ref. B with H-slot (Ref. C) (d) Ref. C with five circular slots (Proposed design).

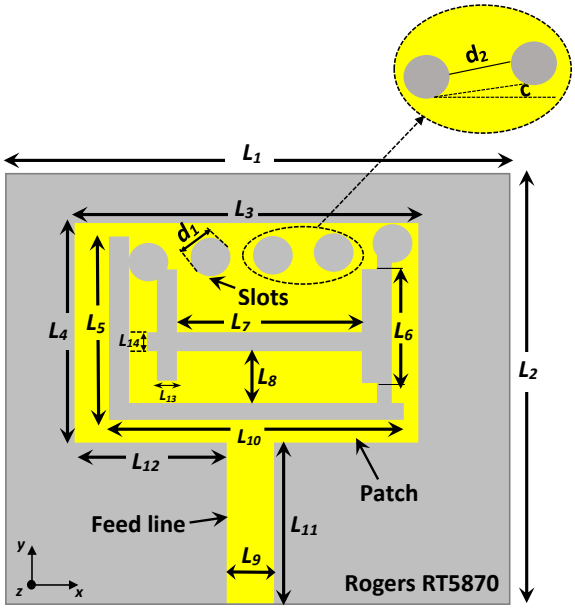


Fig. 2: Geometry of the proposed self-isolated 5G mm-wave antenna.

TABLE I: Dimensions of the self-isolated Antenna Array

| Parameters | $L_1$ | $L_2$ | $L_3$ | $L_4$ | $L_5$ | $L_6$ | $L_7$ | $L_8$ |
|---|---|---|---|---|---|---|---|---|
| Values (mm) | 10 | 12 | 6.5 | 4 | 3.5 | 2.0 | 3.64 | 1.24 |
| Parameters | $L_9$ | $L_{10}$ | $L_{11}$ | $L_{12}$ | $L_{13}$ | $L_{14}$ | $d_1$ | $d_2$ |
| Values (mm) | 1.11 | 5.75 | 3.9 | 2.86 | 0.36 | 0.25 | 0.78 | 0.45 |

### B. Wide Band and Self-isolation mechanism

Herein, we explain the self-isolation technique employing the surface current distributions. In addition, we demonstrate how the different incorporated slots can simultaneously increase the matching bandwidth as well as increase the isolation in a MIMO array configuration.

It is well known that microstrip patch antennas are very effective because of their simple, robust, and compact structure.

However, microstrip antennas are limited by low bandwidth, gain, and surface waves [4]. According to [30], the surface wave is predominant in a microstrip antenna if the normalized substrate electrical thickness $h/\lambda_0$ is equal to or higher than:

$$\frac{h}{\lambda_0} = \frac{0.3}{2\pi\sqrt{\epsilon_r}} \quad (1)$$

where $h$ is the substrate thickness, $\lambda_0$ is the wavelength in free space, and $\epsilon_r$ is the dielectric constant of the substrate. Substituting the parameters of our antenna in (1), the left side and right side of the equation are approximately 0.06 and 0.03, respectively. Therefore, it is clear that the surface wave is responsible for the coupling in this antenna.

One way to improve the impedance bandwidth of the antenna is through the use of slots [31]. Slots enable more resonant modes to be excited in the patch by interrupting the uniformity of the patch, thereby, inducing perturbations, counteract or constrain EM waves. This will disturb the surface current distribution in the patch, resulting in multiple resonances being excited in the patch. The EM wave propagation can be effectively controlled by meticulously optimizing the slots dimensions and locations, which can eventually alter the inductive and capacitive response of the entire patch. The dimensions and locations of the slots were chosen by carefully observing the current paths on the surface of the antenna. The disturbed surface current introduced due to the slots is responsible for the increase in the isolation between the antenna elements when the positions and dimensions of the slots are carefully optimized. To ascertain the impedance bandwidth improvement and isolation enhancement capability of the slots, the antenna is arranged in a $1\times2$ configuration, as shown in Fig. 3 with dimension $L_{15}$ = 19 mm X $L_{16}$ = 12 m, and edge-to-edge separation of $d$ = 0.2 mm, which is approximately $0.023\lambda_0$ at 35 GHz.

Fig. 4 depicts the reflection and transmission coefficients of the reference antenna (Ref. A), Ref. B, Ref. C and the proposed antenna shown in Fig. 1. It is clear that the reference antenna (Ref. A) has a limited bandwidth between 37-40 GHz with a transmission coefficient of -11 dB at 38 GHz. By carefully introducing the U-slot on the patch at an appropriate distance (see Ref. B in Fig. 1), the impedance bandwidth of the antenna is reduced with a resonance around 39 GHz as shown in Fig. 4a, while the isolation increases to about -22 dB as seen in Fig. 4b. To further increase the impedance bandwidth and mutual isolation, another H-slot is inserted at $L_8$ from the U-slot as shown in Ref. C of Fig. 1 and the antenna geometry of Fig. 2. The combination of U- and H-slot slots alters the mean current path of the antenna, which consequently disturbs the current distribution on the patch, thereby, generating more resonances and improves the isolation. Clearly, the results of Fig. 4 show that the working bandwidth of the Ref. C antenna has been significantly enhanced to include dual bands of 30-35 GHz and 36.5-42 GHz with maximum isolation of -50 dB.

To enable the antenna work over a wider bandwidth, five circular slots are meticulously optimized and incorporated into the patch (see proposed in Figs. 1d and 2). It is clear from Fig. 4 that the antenna now resonates from 30-41 GHz with a maximum isolation improvement of 67 dB at 33.2 GHz

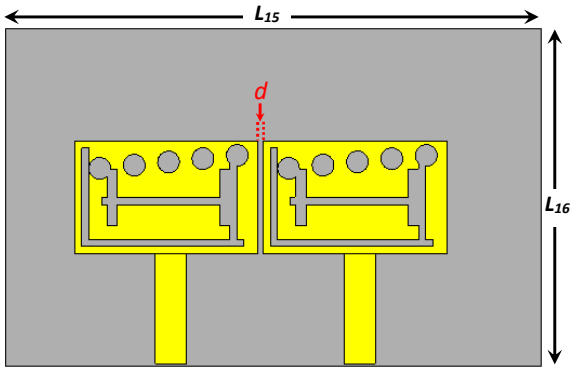


Fig. 3: $1\times2$ MIMO array configuration of the self-isolated 5G mm-wave antenna ($d$ = 2 mm).

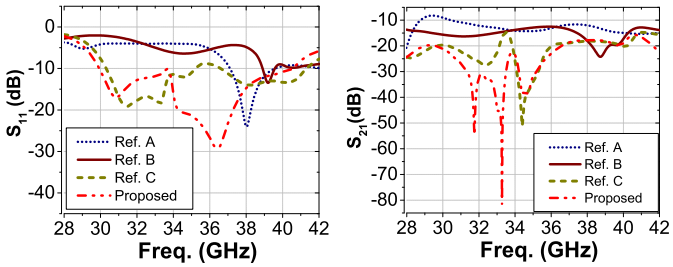


(a) (b)

Fig. 4: (a) $S_{11}$ and (b) $S_{21}$ throughout the antenna evolution from the reference $1\times2$ antenna array (Ref. A) to the proposed $1\times2$ self-isolated antenna array.

compared to the reference antenna (Ref. A). It is worthy of note that the major contributor to the coupling reduction and bandwidth enhancement is the carefully placed H-slot in addition to the U-slot and circular slots. Figure 5 shows a good agreement between the simulated and measured $S_{11}$, $S_{22}$, and $S_{21}$ of the reference $1\times2$ array (Ref. A) and the proposed $1\times2$ self-isolated antenna array.

Figure 6 clearly shows the surface current distribution of the antenna evolution. The surface current reduces as we move from Ref. A to the proposed antenna because of the meticulously optimized slots etched off the antenna. It is also evident that the surface currents are trapped around the slots as the number of slots increases, thereby, preventing most of the surface currents from reaching the other antenna element. This leads to inevitable increase in isolation. Comparing Fig. 6a (Ref. A) and Fig. 6d (Proposed), the decrease in the surface current around and between the antenna elements is obvious. Therefore, introducing the rigorously optimized U-slot, H-slot slot and five circular slots improves the bandwidth, and isolation of the mm-wave patch antenna *without* the need for any decoupling structure. The effect of changing the number of circular slots and some key features of the MIMO antenna array is discussed in the following subsection.

### C. Parametric analyses

This subsection highlights the results obtained by a rigorous tuning of some key parameters of the antenna to improve its

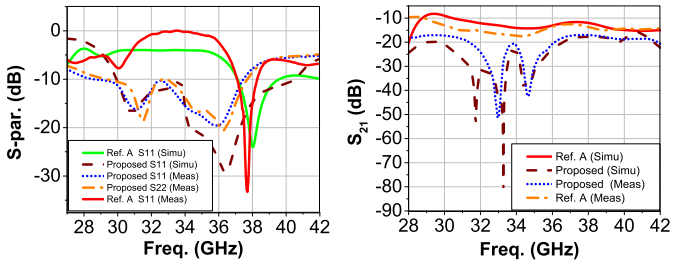


(a) (b)

Fig. 5: Measured and simulated (a) $S_{11}$-$S_{22}$, and (b) $S_{21}$ of the reference 1×2 array (Ref. A) and the proposed 1×2 self-isolated antenna array.

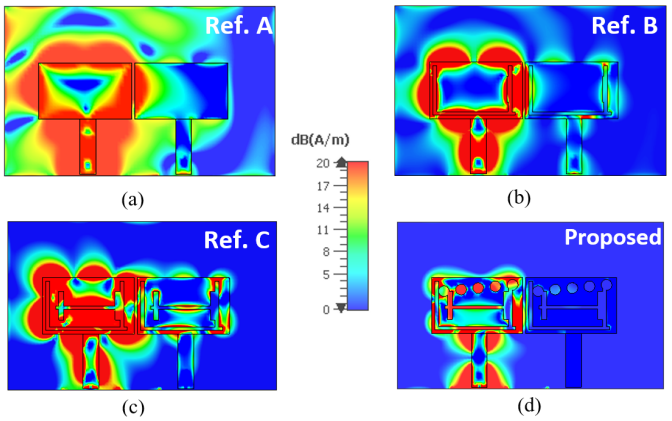


(a) (b) (c) (d)

Fig. 6: Surface current distribution depicting the design evolution of the proposed 1×2 self-isolated antenna array at 33 GHz: (a) No slots (Ref. A) (b) Ref. A with U-slot (Ref. B) (c) Ref. B with H-slot (Ref. C) (d) Ref. C with five circular slots (Proposed).

overall performance. The parameters and dimensions of the antenna in Figs. 2 and 3 are tuned and the results are discussed. Fig. 7a illustrates the effect of changing the edge-to-edge distance on the isolation characteristics while keeping other parameters constant. The isolation increases as the distance between the two antennas increases. However, the smallest distance chosen in this work ($d$ = *0.2 mm*) still exhibits very good isolation less than 20 dB throughout the working bandwidth, which fulfills MIMO isolation requirements. The reflection coefficient is not affected by the change of the inter-element spacing, hence, not shown. Fig. 7b depicts the effect of the number of circular slots on the S-parameters while keeping other parameters constant. The proposed antenna with five slots exhibits the best reflection and transmission characteristics over the 30-41 GHz impedance bandwidth.

Fig. 8a depicts that $L_8$ = 1.24 mm (see Fig. 2) is the best position to place the H-slot above the U-slot to obtain the desired reflection and transmission characteristics. Furthermore, Fig. 8b shows that the optimum rectangular slot width $L_{14}$ to obtain the best reflection and isolation characteristics is 0.25 mm, while other parameters are unaltered.

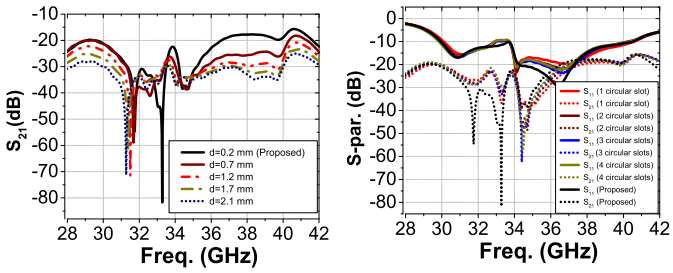


(a) (b)

Fig. 7: Effect of changing (a) the inter-element distance ($d$), and (b) the number of circular slots, on the S-parameters of the proposed 1×2 self-isolated 5G mm-wave antenna.

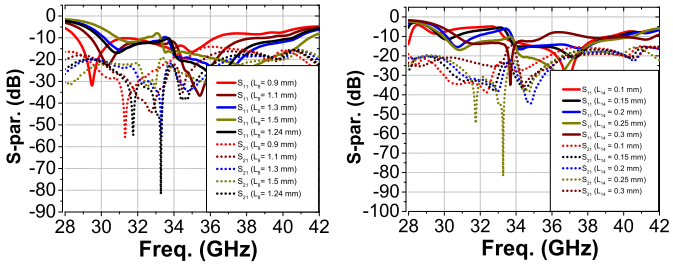


(a) (b)

Fig. 8: Effect of changing (a) $L_8$, and (b) rectangular slot width ($L_{14}$), on the S-parameters of the proposed self-isolated 1×2 5G mm-wave antenna.

### D. *Far-field properties*

Fig. 9 plots the simulated radiation patterns of the proposed self-isolated 1×2 5G mm-wave antenna compared with the reference array (Ref. A) in the E- and H-planes at 31, 35, and 38 GHz. After inserting the slots and as a result of the surface current reduction, the radiation patterns of the array become more directive along the broadside direction over the frequency band of interest. Furthermore, a slight beam deflection is observed at 38 GHz, which is expected, because of the high bandwidth of the antenna. A good agreement between the simulated and measured radiation patterns of the proposed self-isolated mm-wave 1×2 antenna at 31, 35, and 38 GHz is depicted in Fig. 10. Fig. 11a shows the fabricated prototypes of the Ref. A, 1×2, and 1×4 MIMO antennas. Fig. 11b shows the radiation patterns measurements set-up in an anechoic chamber.

## III. MIMO Antenna Configuration

To verify the MIMO capability of the proposed antenna, a 4-element array is designed and arranged along the x-axis (H-plane) as shown in Fig. 12 with an edge-to-edge distance of $d$ = *0.2 mm*. The simulated surface current distribution of the 1×4 antenna when one port is excited, and the others are terminated with a matched load at 33 GHz is shown in Fig. 13. Fig. 13a shows that the surface current diminishes as the distance between the excited antenna (Ant.1) and the other antennas increases. Ant. 4 has almost no surface current when Ant. 1 is excited. Additionally, when Ant. 2 is excited, Ant.

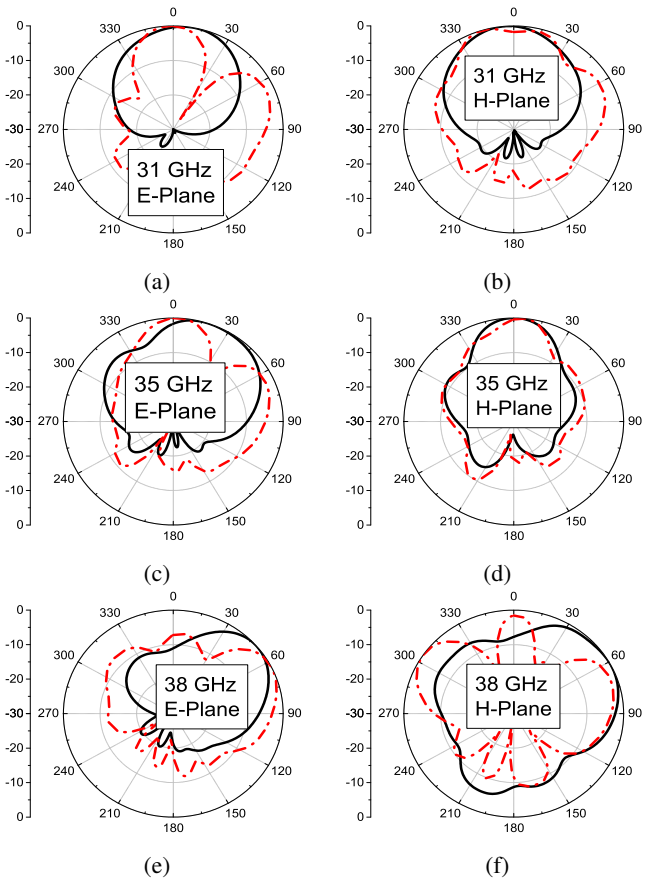


Fig. 9: Simulated radiation patterns of the proposed self-isolated 1×2 5G mm-wave antenna (solid) compared with the Ref. (A) array (dashed) at 31, 35, and 38 GHz.

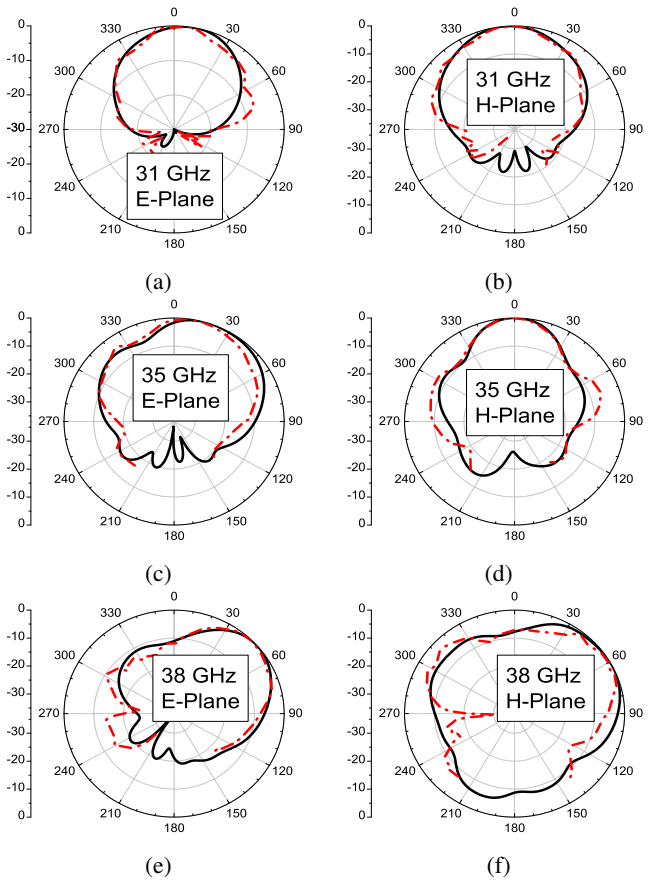


Fig. 10: Measured (dashed) and simulated (solid) radiation patterns of the proposed self-isolated 1×2 5G mm-wave antenna at 31, 35, and 38 GHz.

1 and Ant. 3 exhibit nearly the same small surface current distribution, while Ant. 4 reveals minimal surface current, as shown in Fig. 13b. The same phenomenon is observed when Ant. 3 or Ant. 4 are excited, as shown in Figs. 13c and 13d. This shows the effectiveness of the added slots in mitigating the surface currents.

The measured and simulated S-parameters of the 1×4 MIMO antenna are depicted in Fig. 14. It is apparent that the reflection coefficient of the antenna remains almost the same for all the four elements while the coupling effects are mostly below -20 dB throughout the desired impedance bandwidth of 30-41 GHz, demonstrating very good MIMO isolation properties.

The measured and simulated E- and H-plane radiation patterns of the 1×4 MIMO array at 32 GHz are depicted in Fig. 15. The MIMO array exhibits consistent broadside radiation characteristics in both planes with almost no beam deflection.

Fig. 16a depicts that the 1×2 antenna array peak gain has been improved compared to the reference antenna (Ref. A) without slots, owing to the isolation improvement over the working bandwidth. It is worth noting that the gain is not improved around 34 GHz due to the low isolation improvement observed around 34 GHz, as seen in Fig. 5b.

The simulated radiation efficiency of the 1×2 antenna array

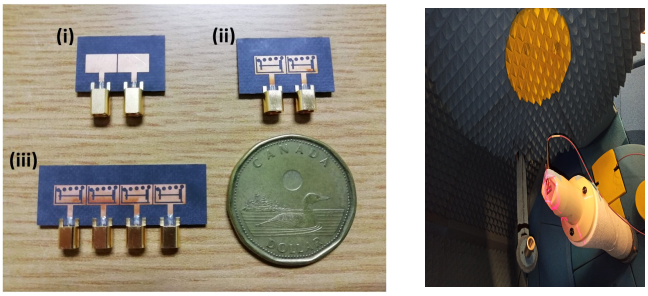


Fig. 11: (a) Fabricated antennas: (i) Ref. A (ii) 1×2, (iii) 1×4 MIMO arrays (b) Radiation pattern measurements set-up.

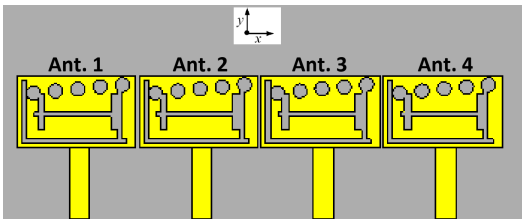


Fig. 12: 1×4 MIMO configuration of the proposed self-isolated 5G mm-wave antenna.

TABLE II: Performance of the proposed mm-wave antenna compared with recent literature

| Year/Ref. | Type of Antenna | Edge-to-edge spacing | Method of decoupling | Impedance bandwidth (%) | Peak Efficiency (%) | Peak Gain (dB) | Maximum isolation improvement |
|---|---|---|---|---|---|---|---|
| 2017 [7] | DRA | $0.5\lambda_0$ | metasurface | 57-64 GHz (11.6%) | 91 | 7.9 | 31.5 dB |
| 2018 [8] | printed patch | $0.67\lambda$ | CSRR | 24.5-25.5 GHz (4%) | - | - | 31.8 dB |
| 2019 [11] | DRA | $0.5\lambda_0$ | hybrid isolator | 50-65 GHz (26.1%) | 69 | 8.1 | 33 dB |
| 2019 [12] | DRA | $0.11\lambda_0$ | metallic vias | 25.1-27 GHz (7.3%) | - | 6.4 | 30 dB |
| 2017 [13] | DRA | $0.12\lambda_0$ | metallic strip | 27.5-28.35 GHz (3%) | - | 10 | 12 dB |
| 2019 [23] | printed patch | $0.014\lambda_0$ | self-isolation | 3.4-3.6 GHz (5.7%) | 58 | - | 17 dB |
| 2018 [25] | Inverted-F | $0.0735\lambda_0$ | self-isolation | 2.4-2.8 GHz (15.4%) | 60 | - | 27 dB |
| 2020 [29] | printed patch | $0.5\lambda_0$ | self-isolation | 3.4-3.6 GHz (5.7%) | - | 7.5 | 37 dB |
| 2020 [32] | printed patch | $0.1\lambda_0$ | EBG, CSRR and DGS | 3.1-3.4 GHz (9.2%) | - | 4.9 | 12 dB |
| Proposed | printed patch | $0.023\lambda_0$ | self-isolation | 28-37.5 GHz (29%) | 96 | 9.6 | 35 dB |

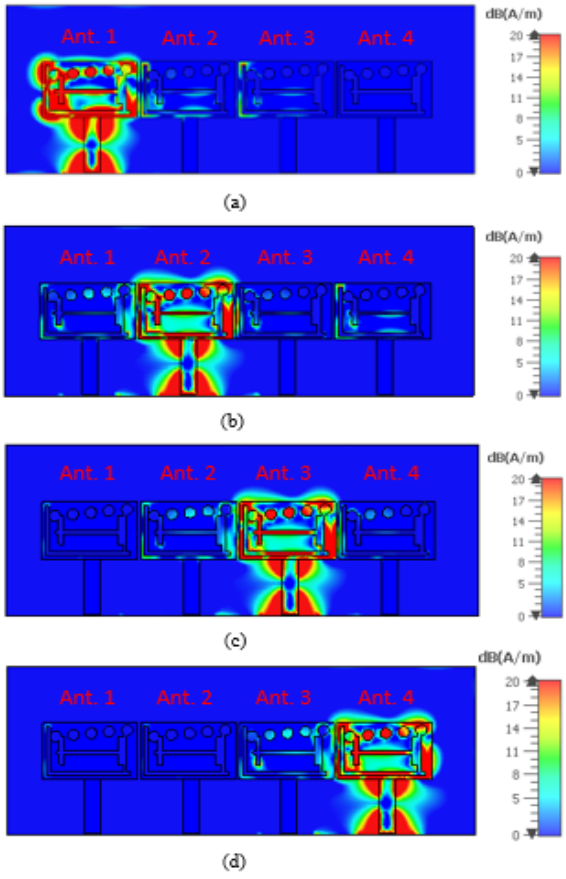


Fig. 13: Surface current distribution of the $1\times4$ MIMO configuration of the proposed self-isolated 5G mm-wave antenna at 33 GHz when (a) Ant.1, (b) Ant. 2, (c) Ant. 3, and (d) Ant. 4 is excited.

is shown in Fig. 16b. As expected, the radiation efficiency has an average value of about 95% compared with 93% of the reference antenna (Ref. A). The efficiency increase is mainly due to the isolation enhancement of the antenna. The efficiency is also observed to be slightly lower around 34 GHz due to the minimal isolation improvement at this frequency, as seen in Fig. 5b.

The Envelope correlation coefficient (ECC) is an important

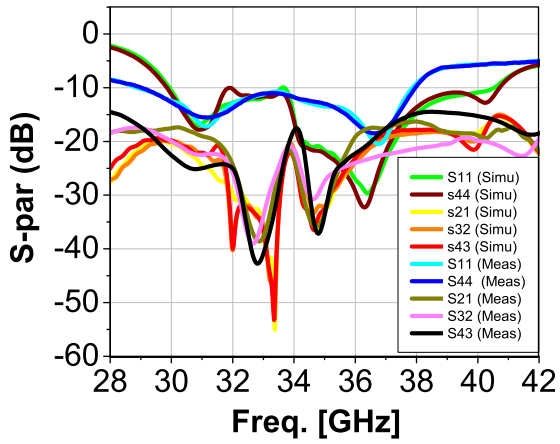


Fig. 14: S-parameters of the $1\times4$ MIMO array configuration of the proposed self-isolated 5G mm-wave antenna.

performance criterion in MIMO antennas. It can be determined using S-parameters or far-field characteristics. The S-parameter method is useful when the efficiency is considerably high [33]. ECC based on S-parameters can be expressed by [34]:

$$ECC = \frac{|S_{11}{}^{*}\ S_{12} + S_{21}{}^{*}\ S_{22}|^2}{|(1-|S_{11}{}^2| - |S_{21}{}^2|)(1-|S_{12}{}^2| - |S_{22}{}^2|)|} \quad (2)$$

The simulated ECC of the reference (Ref. A) and the proposed $1\times2$ array, based on S-parameters, is depicted in Fig. 17a. The proposed MIMO antenna array exhibits ECC lower than -20 dB throughout the operational bandwidth, with a considerable coupling reduction compared with the Ref. A antenna, indicating an isolation improvement. The diversity gain is another important parameter for MIMO system evaluation, and it can be obtained using [34]:

$$Diversity\ gain = 10\sqrt{1-|\ ECC\ |} \quad (3)$$

Where 10 is the apparent maximum diversity gain. The ECC of the proposed antenna is less than 0.01, thereby, making its diversity gain around 10 dB within the operational bandwidth as depicted in Fig. 17b. This improved diversity gain is a result of the surface wave suppression.

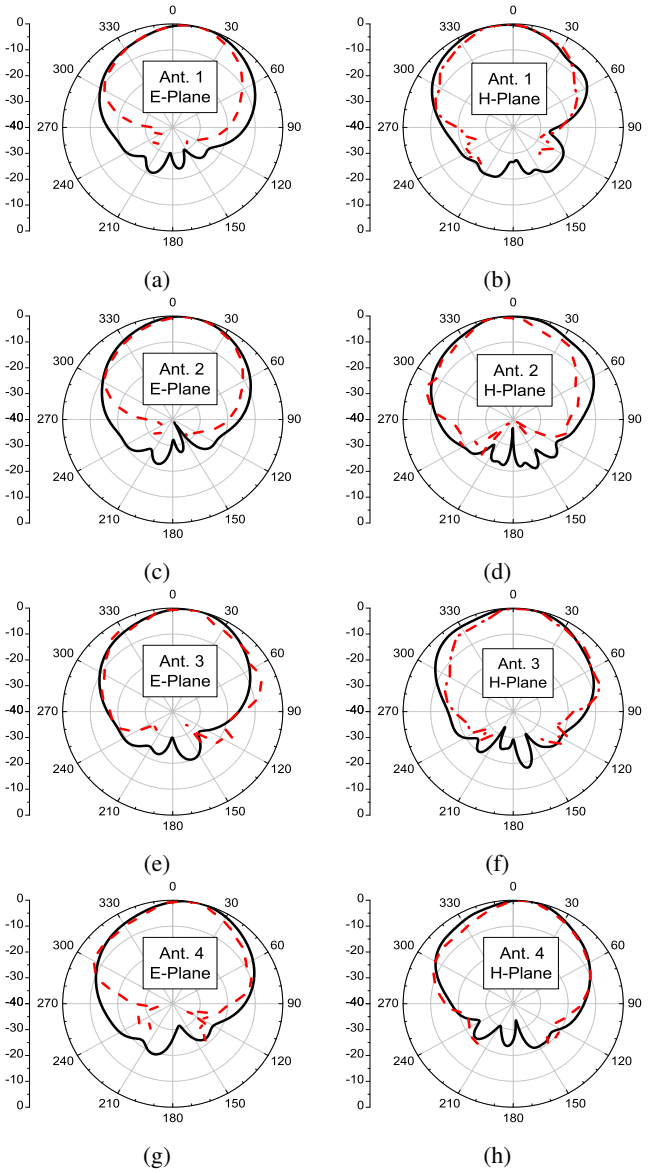


Fig. 15: Measured (dashed) and simulated (solid) radiation patterns of the $1\times4$ MIMO configuration of the proposed self-isolated 5G mm-wave antenna at 32 GHz.

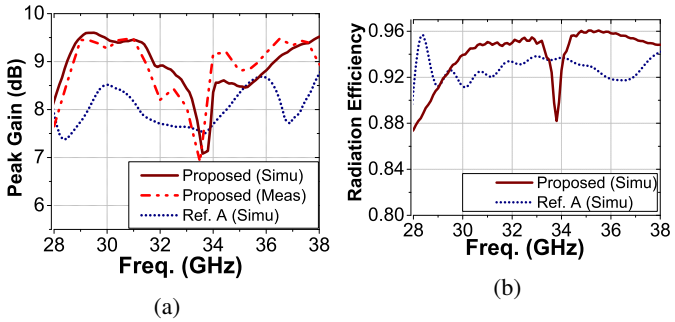


Fig. 16: (a) Peak gain and (b) Radiation efficiency, of the proposed self-isolated $1\times2$ mm-wave 5G antenna compared with the reference antenna (Ref. A).

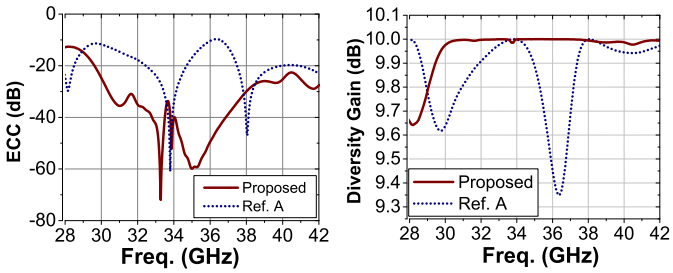


Fig. 17: (a) Envelope correlation coefficient (ECC). (b) Diversity gain of the $1\times2$ self-isolated 5G mm-wave antenna compared with the reference antenna.

Table II depicts the comparison of the proposed antenna with recent literature. The proposed antenna exhibits the largest impedance bandwidth *combined* with high efficiency, gain, and maximum isolation improvement with minimal edge-to-edge spacing. The proposed antenna is the only design in Table II that acquires all these attractive features simultaneously without compromising any fundamental design objective.

## ACKNOWLEDGEMENT

## IV. CONCLUSION

A novel, simple and low-cost self-isolated mm-wave MIMO 5G antenna with impedance bandwidth of 28-37.5 GHz, 51 dB maximum isolation, and edge-to-edge spacing of $0.023\lambda_0$ has been presented. No additional or external isolating structures have been used. Various antenna parameters have been investigated to achieve high bandwidth and the smallest possible edge-to-edge spacing. Moreover, a $1\times4$ MIMO configuration of the antenna has been presented and analyzed. Good agreement between measured and simulated results has been achieved. The proposed MIMO antenna exhibited a wide bandwidth, improved efficiency, minimal envelope correlation coefficient, and significant isolation improvement with minimal inter-element spacing compared to previously published designs. The proposed work is the first to develop a simple, low-cost self-isolated MIMO antenna system at the mm-wave 5G frequency range.

## REFERENCES

[1] J. G. Andrews, S. Buzzi, W. Choi, S. V. Hanly, A. Lozano, A. C. K. Soong, and J. C. Zhang, "What will 5G be?" *IEEE Journal on Selected Areas in Communications*, vol. 32, no. 6, pp. 1065–1082, June 2014.

[2] W. Hong, "Solving the 5G mobile antenna puzzle: Assessing future directions for the 5G mobile antenna paradigm shift," *IEEE Microwave Magazine*, vol. 18, no. 7, pp. 86–102, Nov 2017.

[3] X. Shen, Y. Liu, L. Zhao, G. Huang, X. Shi, and Q. Huang, "A miniaturized microstrip antenna array at 5G millimeter-wave band," *IEEE Antennas and Wireless Propagation Letters*, vol. 18, no. 8, pp. 1671–1675, Aug 2019.

[4] S. F. Jilani and A. Alomainy, "Millimetre-wave t-shaped MIMO antenna with defected ground structures for 5G cellular networks," *IET Microwaves, Antennas Propagation*, vol. 12, no. 5, pp. 672–677, 2018.

[5] J. Qiang, F. Xu, and W. Fan, "Reducing mutual coupling of millimeter wave array antennas by fractal defected ground structure," in *2018 12th International Symposium on Antennas, Propagation and EM Theory (ISAPE)*, Dec 2018, pp. 1–3.

[6] S. Gupta, Z. Briqech, A. R. Sebak, and T. Ahmed Denidni, "Mutual-coupling reduction using metasurface corrugations for 28 GHz MIMO applications," *IEEE Antennas and Wireless Propagation Letters*, vol. 16, pp. 2763–2766, 2017.

[7] A. Dadgarpour, B. Zarghooni, B. S. Virdee, T. A. Denidni, and A. A. Kishk, "Mutual coupling reduction in dielectric resonator antennas using metasurface shield for 60-GHz MIMO systems," *IEEE Antennas and Wireless Propagation Letters*, vol. 16, pp. 477–480, 2017.

[8] R. Selvaraju, M. H. Jamaluddin, M. R. Kamarudin, J. Nasir, and M. H. Dahri, "Mutual coupling reduction and pattern error correction in a 5G beamforming linear array using csrr," *IEEE Access*, vol. 6, pp. 65 922–65 934, 2018.

[9] S. I. Naqvi, A. H. Naqvi, F. Arshad, M. A. Riaz, M. A. Azam, M. S. Khan, Y. Amin, J. Loo, and H. Tenhunen, "An integrated antenna system for 4G and millimeter-wave 5G future handheld devices," *IEEE Access*, vol. 7, pp. 116 555–116 566, 2019.

[10] R. Karimian, A. Kesavan, M. Nedil, and T. A. Denidni, "Low-mutual-coupling 60-GHz MIMO antenna system with frequency selective surface wall," *IEEE Antennas and Wireless Propagation Letters*, vol. 16, pp. 373–376, 2017.

[11] M. Al-Hasan, I. Ben Mabrouk, E. R. F. Almajali, M. Nedil, and T. A. Denidni, "Hybrid isolator for mutual-coupling reduction in millimeter-wave MIMO antenna systems," *IEEE Access*, vol. 7, pp. 58 466–58 474, 2019.

[12] Y. M. Pan, X. Qin, Y. X. Sun, and S. Y. Zheng, "A simple decoupling method for 5G millimeter-wave MIMO dielectric resonator antennas," *IEEE Transactions on Antennas and Propagation*, vol. 67, no. 4, pp. 2224–2234, April 2019.

[13] Y. Zhang, J. Deng, M. Li, D. Sun, and L. Guo, "A MIMO dielectric resonator antenna with improved isolation for 5G mm-wave applications," *IEEE Antennas and Wireless Propagation Letters*, vol. 18, no. 4, pp. 747–751, April 2019.

[14] S. Gaya, O. Sokunbi, A. Hamza, S. I. M. Sheikh, and H. Attia, "Multiple-input-multiple-output antenna with pattern reconfiguration and correlation reduction for wlan applications," *Engineering Reports*, vol. 2, no. 12, p. e12272, 2020.

[15] S. Zhu, H. Liu, Z. Chen, and P. Wen, "A compact gain-enhanced vivaldi antenna array with suppressed mutual coupling for 5G mmwave application," *IEEE Antennas and Wireless Propagation Letters*, vol. 17, no. 5, pp. 776–779, May 2018.

[16] T. H. Jang, H. Y. Kim, D. M. Kang, S. H. Kim, and C. S. Park, "60 GHz low-profile, wideband dual-polarized u-slot coupled patch antenna with high isolation," *IEEE Transactions on Antennas and Propagation*, vol. 67, no. 7, pp. 4453–4462, July 2019.

[17] M. J. Al-Hasan, T. A. Denidni, and A. R. Sebak, "Millimeter-wave compact EBG structure for mutual coupling reduction applications," *IEEE Transactions on Antennas and Propagation*, vol. 63, no. 2, pp. 823–828, Feb 2015.

[18] O. Sokunbi and H. Attia, "Highly reduced mutual coupling between wideband patch antenna array using multiresonance EBG structure and defective ground surface," *Microwave and Optical Technology Letters*, vol. 62, no. 4, pp. 1628–1637, 2020.

[19] O. Sokunbi, H. Attia, and S. I. Sheikh, "Microstrip antenna array with reduced mutual coupling using slotted-ring EBG structure for 5G applications," in *2019 IEEE International Symposium on Antennas and Propagation and USNC-URSI Radio Science Meeting*, July 2019, pp. 1185–1186.

[20] D. Gao, Z. X. Cao, S. D. Fu, X. Quan, and P. Chen, "A novel slot-array defected ground structure for decoupling microstrip antenna array," *IEEE Transactions on Antennas and Propagation*, vol. 68, no. 10, pp. 7027–7038, 2020.

[21] B. Niu and J. Tan, "Compact self-isolated MIMO antenna system based on quarter-mode siw cavity," *Electronics Letters*, vol. 55, no. 10, pp. 574–576, 2019.

[22] Y. Li, C. Sim, Y. Luo, and G. Yang, "High-isolation 3.5 GHz eight-antenna MIMO array using balanced open-slot antenna element for 5G smartphones," *IEEE Transactions on Antennas and Propagation*, vol. 67, no. 6, pp. 3820–3830, June 2019.

[23] Z. Ren, A. Zhao, and S. Wu, "MIMO antenna with compact decoupled antenna pairs for 5G mobile terminals," *IEEE Antennas and Wireless Propagation Letters*, vol. 18, no. 7, pp. 1367–1371, July 2019.

[24] A. Zhao and Z. Ren, "Multiple-input and multiple-output antenna system with self-isolated antenna element for fifth-generation mobile terminals," *Microwave and Optical Technology Letters*, vol. 61, no. 1, pp. 20–27, 2019.

[25] J. Sui and K. Wu, "Self-curing decoupling technique for two inverted-f antennas with capacitive loads," *IEEE Transactions on Antennas and Propagation*, vol. 66, no. 3, pp. 1093–1101, March 2018.

[26] K.-L. Wong, C.-C. Wan, and L.-Y. Chen, "Self-decoupled compact metal-frame lte MIMO antennas for the smartphone," *Microwave and Optical Technology Letters*, vol. 60, no. 5, pp. 1170–1179, 2018.

[27] L. Sun, Y. Li, Z. Zhang, and H. Wang, "Self-decoupled MIMO antenna pair with shared radiator for 5G smartphones," *IEEE Transactions on Antennas and Propagation*, vol. 68, no. 5, pp. 3423–3432, 2020.

[28] A. Zhao and Z. Ren, "Size reduction of self-isolated MIMO antenna system for 5G mobile phone applications," *IEEE Antennas and Wireless Propagation Letters*, vol. 18, no. 1, pp. 152–156, Jan 2019.

[29] H. Lin, Q. Chen, Y. Ji, X. Yang, J. Wang, and L. Ge, "Weak-field-based self-decoupling patch antennas," *IEEE Transactions on Antennas and Propagation*, vol. 68, no. 6, pp. 4208–4217, 2020.

[30] M. M. Nikolic, A. R. Djordjevic, and A. Nehorai, "Microstrip antennas with suppressed radiation in horizontal directions and reduced coupling," *IEEE Transactions on Antennas and Propagation*, vol. 53, no. 11, pp. 3469–3476, 2005.

[31] S. T. Fan, Y. Z. Yin, B. Lee, W. Hu, and X. Yang, "Bandwidth enhancement of a printed slot antenna with a pair of parasitic patches," *IEEE Antennas and Wireless Propagation Letters*, vol. 11, pp. 1230–1233, 2012.

[32] Z. Yang, J. Xiao, and Q. Ye, "Enhancing MIMO antenna isolation characteristic by manipulating the propagation of surface wave," *IEEE Access*, vol. 8, pp. 115 572–115 581, 2020.

[33] M. A. Jensen and J. W. Wallace, "A review of antennas and propagation for MIMO wireless communications," *IEEE Transactions on Antennas and Propagation*, vol. 52, no. 11, pp. 2810–2824, 2004.

[34] J. Park, M. Rahman, and H. N. Chen, "Isolation enhancement of wide-band MIMO array antennas utilizing resistive loading," *IEEE Access*, vol. 7, pp. 81 020–81 026, 2019.